Potential of hydrogenated microcrystalline silicon-germanium for low thermal budget near infrared sensors

Alestair Wilson, Bilel Saidi, Mickael Gros-Jean, Jean-Gabriel Mattei, Benjamin Fornacciari, Erwann Fourmond

Potential of hydrogenated microcrystalline silicon-germanium for low thermal budget near infrared sensors

Alestair Wilson*[ab], Bilel Saidi[a], Mickaël Gros-Jean[a], Jean-Gabriel Mattei[a], Benjamin Fornacciari[b], Erwann Fourmond[b]

[a]STMicroelectronics, 850 rue Jean Monnet, 38926 Crolles, France; [b]Univ Lyon, INSA Lyon, CNRS, Ecole Centrale de Lyon, Université Claude Bernard Lyon 1, CPE Lyon, INL UMR5270, 69621 Villeurbanne, France

ABSTRACT

Microcrystalline Silicon-Germanium (µc-SiGe:H) is a low bandgap material whose optical and electrical properties strongly depend on deposition conditions. In this work, an above integrated circuit (above-IC) [1]–[3] compatible, near infrared (NIR) sensor based on microcrystalline Silicon-Germanium is produced and characterized. The N-I-P photodiode is obtained by radio frequency plasma enhanced chemical vapor deposition (RF-PECVD) from a SiH_4 + GeH_4 + H_2 gas mixture. Quantum efficiency measurements reveals a 60 at.% Ge fraction is optimal for a 200 nm thick µc-SiGe:H intrinsic absorber layer. Above this threshold, the degradation in electrical properties prevails on the gain in absorption.

Keywords: microcrystalline, silicon-germanium, above-IC, PECVD, photodiode, near infrared

1. INTRODUCTION

The growing internet of things (IoT) market pushes for the development of reliable, low cost sensors. Among these sensors, cheap near infrared CMOS image sensors are needed by the automotive and mobile phone industry. In a "More than Moore" approach to integration, above integrated circuit (above-IC) [1]–[3] CMOS image sensors meet this need for cost effective sensors. This approach however strongly limits the thermal budget for sensor fabrication due to risks of damage and diffusion in the underlying CMOS interconnections [4], [5]. A solution to maintain a low thermal budget (< 350 °C) is to rely on Plasma Enhanced Chemical Vapor Deposition (PECVD), which makes it possible to manufacture a wide range of thin films. Abundant literature can be found concerning amorphous and microcrystalline silicon (a/µc-Si:H), in part due to its use in the solar cells industry [6]–[8]. On the other hand, µc-SiGe:H remains less used and was mostly studied as a low band-gap material for multijunction solar cells [9]–[12]. Such silicon-germanium based alloys have a great potential for optical sensors due to their high optical absorption in the visible to near-infrared spectral range [13]. In this paper, we will focus on the structural and optical properties of µc-SiGe:H thin films deposited by PECVD whose Ge atomic content range from 0 % to 70 %. These materials will then be integrated into a glass / ITO / µc-Si:P / µc-$Si_{1-x}Ge_x$:H / µc-Si:B / Ag stack for optoelectronic characterization.

2. EXPERIMENTAL SECTION

2.1 PECVD and sample preparation

Thin films were deposited using a capacitively coupled 13,56 MHz RF-PECVD (Vision 310, PlasmaTherm). The showerhead-type powered electrode as well as the floating electrode are 300 mm in diameter. Thin film deposition was done at a substrate temperature set to 250 °C for all samples. The substrate used were glass (soda lime, from Ossila), monocrystalline silicon (100 oriented, $\rho = 200\ \Omega \cdot cm$) and ITO coated glass (Ossila). The glass substrates were cleaned using ultrasonic bath in an ethanol solution at 40 °C and rinsed with deionized (DI) water while silicon was deoxidized in a 5% HF solution before being rinsed with DI water. The ITO coated substrates were cleaned identically to the glass substrate, with an additional ozone surface treatment for the ITO activation.

*alestair.wilson@insa-lyon.fr; phone +33 660111940; inl.cnrs.fr

2.2 N-I-P photodiode structure and fabrication

Prototype photodiodes shown in Figure 1 were based on a N-I-P structure (µc-Si:P / µc-$Si_{1-x}Ge_x$:H / µc-Si:B) deposited by PECVD in a single process step. ITO coated glass was used as a transparent conductive substrate through which light can be shined to reach the active part of the photodiode. The 300 nm thick Ag anode (on µc-Si:B) and cathode (on ITO) were deposited on ITO and µc-Si:B by sputtering at room temperature to avoid any accidental recrystallization of the deposited layers.

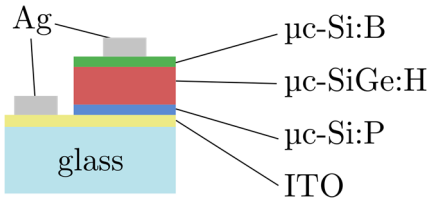

Figure 1: Schematic diagram of the photodiode prototype structure, based on a glass / ITO / µc-Si:P / µc-$Si_{1-x}Ge_x$:H / µc-Si:B / Ag stack. The active surface area of the photodiode is defined by the Ag anode area of 6.25 mm^2.

All µc-$Si_{1-x}Ge_x$:H thin films were deposited under similar conditions from a SiH_4 + GeH_4 + H_2 gas mixture. Temperature, power, pressure and total gas flow rate Φ_{tot} were kept constant at 250 °C, 50 W, 1 Torr and 500 sccm, respectively. The hydrogen dilution factor R_H was set to 100. It is defined as the ratio of hydrogen to precursor gas flow rate in sccm ($R_H = \Phi_{H2}/[\Phi_{SiH4} + \Phi_{GeH4}]$). The GeH_4 to SiH_4 ratio was adapted for each sample to reach the desired Germanium composition x_{Ge}. Doped microcrystalline silicon (µc-Si:H) used as n and p-type layers in N-I-P photodiode structures were deposited from a SiH_4 + PH_3 + H_2 or SiH_4 + B_2H_6 + H_2 gas mixture, thus obtaining a n-type µc-Si:P or a p-type µc-Si:B layer. The deposition conditions and corresponding carrier concentration measured by Hall effect can be found in Table 1. Phosphorus doped microcrystalline silicon deposition and characterization was extensively studied in a previous paper [14].

Table 1: Doped microcrystalline silicon deposition conditions. $\beta = \Phi_{PH3}/\Phi_{SiH4}$ is the ratio of doping gas to SiH_4 gas flow rate.

Layer	Dop. gas	β	t_{dep}	R_H	Temp.	Power	Press.	Φ_{tot}	n / p
	–	–	[min]	–	[°C]	[W]	[mTorr]	[sccm]	[cm^{-3}]
µc-Si:P	PH_3	0.05%	18	50	250	30	800	350	1.1e+19
µc-Si:B	B_2H_6	0.05%	18	50	250	30	800	350	3.4e+18

2.3 Characterization techniques

Film thickness and structural properties of the film were obtained from Scanning transmission electron microscope (STEM) images of lamellae extracted by Focused ion beam (FIB) milling. Absorption coefficient of the films was obtained from Spectroscopic Ellipsometry (SE) measurements of films deposited on glass, in the 0.6 to 5 eV range (Horiba UVISEL). SE data was fitted using 3 layer model accounting for the glass substrate, the bulk of the material and the surface roughness. A Kato-Adachi dispersion formula [15], [16] was used to describe µc-SiGe:H layers. Raman spectroscopy (Horiba Jobin-Yvon Aramis, 1.1 cm^{-1} resolution) was performed on the samples using a 473 nm laser excitation to obtain structural and chemical information on the films. The Raman spectra of µc-SiGe:H has 3 main peaks corresponding to the Raman shift $\Delta\omega$ of Si-Si, Si-Ge and Ge-Ge bonds, respectively found around 500 cm^{-1}, 400 cm^{-1} and 300 cm^{-1}. The relative intensity, position and broadening of those peaks is directly dependent on crystalline volume fraction and Ge content x_{Ge} [17]–[20]. External quantum efficiency (EQE) was measured in the 300 to 1100 nm spectral range with a 5 nm resolution. The current generated at each wavelength was normalized by the photogenerated current of a reference c-Si photodiode in order for the measurement to be independent of the Xenon light source used. Internal quantum efficiency (IQE) was then obtained by performing reflectometry measurements on the sample in the same spectral range. Thanks to the Ag anode acting as a backside reflector, transmission of light at normal incidence is 0. IQE can thus be expressed as a function of the reflectance $R(\lambda)$:

$$IQE(\lambda) = \frac{EQE(\lambda)}{1 - R(\lambda)} \quad (1)$$

3. RESULTS

3.1 Optical properties of µc-SiGe:H thin films

In order to study the optical properties of the material, approximately 100 nm thick films of µc-SiGe:H with a Ge fraction x_{Ge} ranging from 0 to 60 at.% were deposited on glass and c-Si. Similarly to µc-Si:H deposition, high hydrogen dilution ($R_H = 100$, see Table 1) was used to ensure film crystallization [6], [17], [21], [22]. The microcrystalline nature of the films was verified by Raman scattering of the glass deposited µc-SiGe:H, given in Figure 2. The narrow peaks observed for all samples an indicator of the crystalline phase [18], as a-SiGe:H yields almost 3 indistinguishable peaks [23].The position of the Si-Si peak is, in the case of a highly crystallized material, dependent on x_{Ge} [17]. A comparison of $\Delta\omega_{Si\text{-}Si}$ as a function of x_{Ge} with the data gathered by Carius *et al* [17] revealed the Ge fraction of our films were precise to about 5 at.%

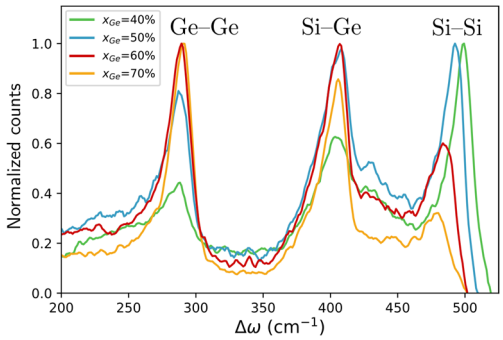

Figure 2: Raman spectra of µc-SiGe:H for x_{Ge} in the 40 to 70 at.% range. The difference in oscillator strength between Si-Si, Si-Ge and Ge-Ge bonds leads to 3 distinct peaks in the case of a crystallized film.

Spectroscopic Ellipsometry measurements were performed on the samples to retrieve the complex refractive index. Up to x_{Ge} = 60 % the data could be fitted with a 3-layer model using the Kato-Adachi formula to described the dielectric function of the material using 11 parameters. This dispersion formula has been used to describe the dielectric function of µc-Si:H [15]. It was thus used for µc-SiGe:H since the dielectric function of c-SiGe closely resembling that of c-Si as long as $x_{Ge} \leq$ 60 %. The extracted absorption coefficient α for the characterized samples is given in Figure 3.

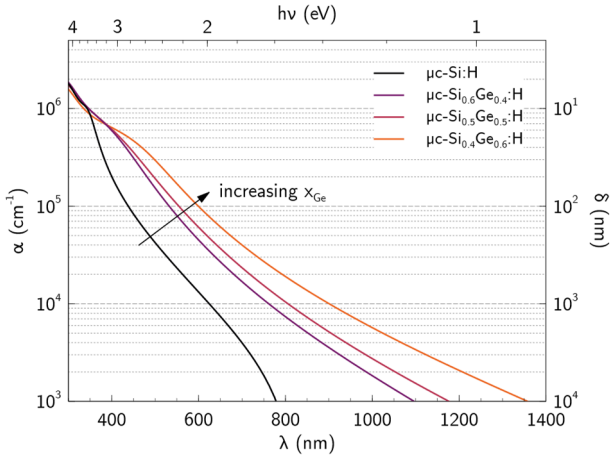

Figure 3: Absorption coefficient α and corresponding absorption depth $\delta = 1/\alpha$ of µc-Si$_{1-x}$Ge$_x$:H obtained by SE in the UV-NIR spectral range for x_{Ge} set to 0 %, 40 %, 50 % and 60 %.

The continuous gain in absorption due to Ge incorporation matches the trend which had been previously observed [13] by transmission-reflection measurements. The sharp drop in absorption of µc-Si:H above 800 nm highlight the limitations of this material for NIR absorption. From this result we expect the photodiodes with a high x_{Ge} for the absorber layer to give a better NIR response if charge transport properties do not decline.

3.2 PIN Photodiode structural characterization

Optoelectronic performance of µc-SiGe:H thin films was tested by integrating them as an absorber layer in a PIN photodiode. The test structure is described above, with the N and P layers made of µc-Si:H. Five devices were produced and tested with a Ge fraction ranging from 0 to 70 %. Deposition time for the absorber layer was adjusted for all samples so the final thickness could remain in the vicinity of 200 nm. Thanks to the Ag back-reflector the optical thickness of the film was roughly equivalent to 400 nm. All the tested samples exhibited a diode behavior in the -1.5 to +1.5 V range under dark conditions.

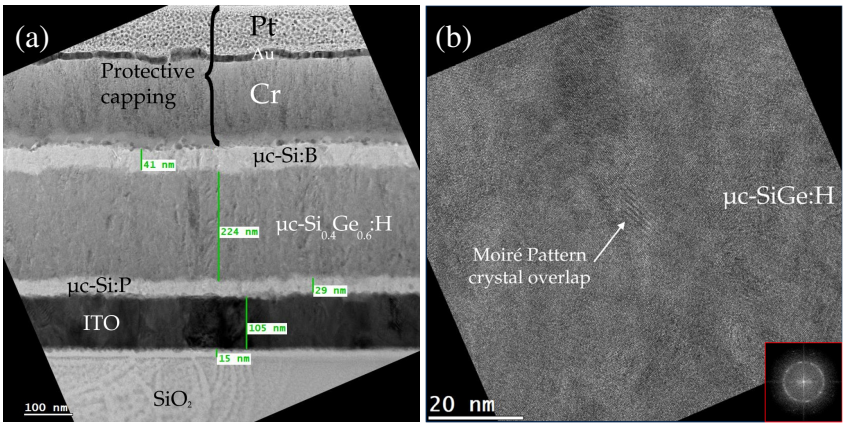

Figure 4: (a) STEM image of the glass / ITO / µc-Si:P / µc-SiGe:H / µc-Si:B stack. The lamella was extracted prior to Ag deposition. (b) STEM close up image of the µc-Si0.4Ge0.6:H absorber layer. The insert in the bottom right corner correspond to the numerical diffraction pattern of the image.

A lamella prepared from the photodiode with a µc-$Si_{0.4}Ge_{0.6}$:H absorber was observed via STEM. The cross section image provided in Figure 4a shows the ITO coated glass on which µc-Si:P, µc-SiGe:H and µc-Si:B were deposited by PECVD. The thickness of the absorber was found to be 224 ± 8 nm thick, with a roughness at the interfaces typical of microcrystalline film growth [6], [24]. In Figure 4b, a close up of the "bulk" of the µc-$Si_{0.4}Ge_{0.6}$:H absorber reveals clear presence of nanometric crystalline domains of about ten nanometers. The numerical diffractogram in the insert of Figure 4b shows a ring patter, characteristic of polycrystals and powders [25]. The period structure seen in the center of the image was attributed to Moiré patterns created from overlapping crystalline orientations in the thickness of the TEM lamella.

3.3 PIN Photodiode optoelectronic characterization

EQE and reflectance spectra were obtained for all five samples in the 300 to 1100 nm range in short circuit conditions. The IQE was then calculated using equation (1). The value obtained for IQE does not account for the parasitic absorption in the doped µc-Si:H or the ITO layer. The results for IQE with increasing Ge fraction are given in Figure 5.

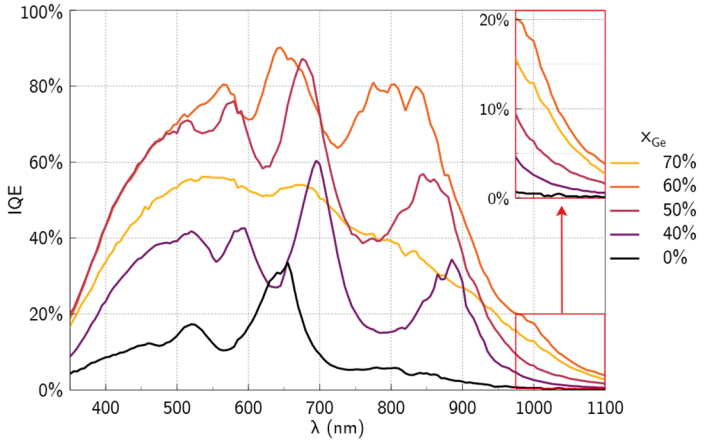

Figure 5: Internal quantum efficiency (IQE) as a function of photon wavelength of an ITO/NIP/Ag photodiode with an absorber layer thickness in the order of 200 nm. The top right insert highlights the IQE for $\lambda = 975$ to 1100 nm.

Oscillations can be seen in the IQE which are most likely a consequence of interferences inside the absorber layer when it becomes semi-transparent. As expected the pure µc-Si:H absorber leads to poor IQE over the whole spectral range due to the layer's thickness and the low absorption coefficient. For µc-SiGe:H absorbers, a high IQE is obtained in the visible range (over 80 % for the best samples). The progressive increase in IQE in the 350 to 500 nm spectral range is due to parasitic absorption in the µc-Si:P layer. In the 800 nm to 1100 nm range, the decrease in IQE can be interpreted as the progressive drop in absorption for our layer, combined to an increasing parasitic absorption by the conductive ITO layer [26].

The optimal value for alloy composition of the absorber was found to be $x_{Ge} = 60$ %. At this composition, the photodiode performs exhibits the best performance throughout the entire spectral range, with IQE($\lambda = 1000$ nm) reaching 17.6 %. As the Ge fraction is increased up to 70 %, the IQE drops although the absorption coefficient should keep increasing.

4. DISCUSSION

The increase in absorption coefficient of µc-SiGe:H with Ge incorporation was found to make NIR sensing feasible with layers as thin as 200 nm. These alloys overcome the weak absorption of µc-Si:H in the NIR range. For the best samples, an IQE higher than 80 % was reached for wavelengths in the visible range. The remaining part of the IQE was lost either due to parasitic absorption or charge carrier recombination. To improve this last point, the band diagram could be engineered by tuning the work function of each material. Parasitic absorption in the NIR could however be addressed by replacing the ITO layer with a more suitable (NIR transparent) TCO.

While one would expect the NIR sensitivity to constantly improve with Ge incorporation, the photodiode with a µc-$Si_{0.3}Ge_{0.7}$:H absorber was found to have lower IQE than the µc-$Si_{0.4}Ge_{0.6}$:H absorber. The degradation occurred over the entire spectral range which suggests the diffusion length in the absorber is becoming noticeably smaller than the absorber thickness. The degradation in electrical properties of µc-SiGe:H films with increasing x_{Ge} was reported by other research groups [13]. With the deposition conditions used in for our samples, the degradation of electrical properties prevailed on optical absorption of the layer above the x_{Ge} = 60 % threshold. This threshold is highly dependent on the chose absorber thickness, other papers thus reported similar drops in QE for x_{Ge} as low as 35 % [9], [27].

The NIR sensitivity in our devices could be improved by increasing absorber thickness and by applying an external reverse bias to the NIP junction. Reverse polarization could increase the extent of the electrical field in the absorber and increase the drift velocity, thus improving charge extraction.

5. CONCLUSION

Photodiodes with increasing Ge fraction for absorber layer were produced and tested in order to find the µc-SiGe:H alloy offering the best compromise between NIR light absorption and charge extraction. The test structure consisted of glass / ITO / µc-Si:P / µc-$Si_{1-x}Ge_x$:H / µc-Si:B / Ag, with x_{Ge} in the 0 – 70 % range. The composition and microcrystalline nature of the deposited thin films was assessed by Raman spectroscopy and STEM imaging. Internal quantum efficiency measurements revealed their sensitivity could extend to 1100 nm with an absorber around 200 nm thick. An optimum for film composition was found with a µc-$Si_{0.4}Ge_{0.6}$:H layer with IQE as high as 17.6 % at λ =1000 nm. Beyond this composition, the degradation in electrical properties of the µc-$Si_{0.3}Ge_{0.7}$:H absorber penalized the IQE in the entire spectral range despite an increase in absorption.

REFERENCES

[1] J. A. Theil, "Advances in elevated diode technologies for integrated circuits: progress towards monolithic instruments," *IEE Proc. - Circuits Devices Syst.*, vol. 150, no. 4, pp. 235–249, Aug. 2003, doi: 10.1049/ip-cds:20030529.

[2] C. Miazza *et al.*, "Performance analysis of a-Si:H detectors deposited on CMOS chips," *MRS Online Proc. Libr.*, vol. 808, no. 1, pp. 269–274, Dec. 2003, doi: 10.1557/PROC-808-A4.46.

[3] J. Schmitz, "Adding functionality to microchips by wafer post-processing," *Nucl. Instrum. Methods Phys. Res. Sect. Accel. Spectrometers Detect. Assoc. Equip.*, vol. 576, no. 1, pp. 142–149, Jun. 2007, doi: 10.1016/j.nima.2007.01.142.

[4] J. Schmitz, “Microchip Post-Processing: There is Plenty of Room at the Top,” in *Future Trends in Microelectronics*, John Wiley & Sons, Ltd, 2013, pp. 110–119. Accessed: Dec. 08, 2022. [Online]. Available: http://onlinelibrary.wiley.com/doi/abs/10.1002/9781118678107.ch8

[5] A. J. Walton *et al.*, “Silicon - Post Processing CMOS Wafers to Create Integrated Sensors, Mems and Electro-Optic Systems,” *SAIEE Afr. Res. J.*, vol. 101, no. 1, pp. 3–10, Mar. 2010, doi: 10.23919/SAIEE.2010.8532213.

[6] A. Matsuda, “Amorphous and Microcrystalline Silicon,” in *Springer Handbook of Electronic and Photonic Materials*, S. Kasap and P. Capper, Eds. Cham: Springer International Publishing, 2017, pp. 573–587. doi: 10.1007/978-3-319-48933-9_25.

[7] B. Kalache, A. I. Kosarev, R. Vanderhaghen, and P. R. i Cabarrocas, “Ion bombardment effects on microcrystalline silicon growth mechanisms and on the film properties,” *J. Appl. Phys.*, vol. 93, no. 2, pp. 1262–1273, Dec. 2002, doi: 10.1063/1.1524707.

[8] S. Hamma, D. Colliquet, and P. R. Cabarrocas, “Microcrystalline Silicon Growth: Deposition Rate Limiting Factors,” *MRS Online Proc. Libr. Arch.*, vol. 507, ed 1998, doi: 10.1557/PROC-507-505.

[9] T. Matsui, C.-W. Chang, T. Takada, M. Isomura, H. Fujiwara, and M. Kondo, “Microcrystalline Si1-xGex Solar Cells Exhibiting Enhanced Infrared Response with Reduced Absorber Thickness,” *Appl. Phys. Express*, vol. 1, no. 3, p. 031501, Mar. 2008, doi: 10.1143/APEX.1.031501.

[10] T. Matsui, K. Ogata, M. Isomura, and M. Kondo, “Microcrystalline silicon–germanium alloys for solar cell application: Growth and material properties,” *J. Non-Cryst. Solids*, vol. 352, no. 9, pp. 1255–1258, Jun. 2006, doi: 10.1016/j.jnoncrysol.2005.11.144.

[11] Y. Cao *et al.*, “Hydrogenated microcrystalline silicon germanium as bottom sub-cell absorber for triple junction solar cell,” *Sol. Energy Mater. Sol. Cells*, vol. 114, pp. 161–164, Jul. 2013, doi: 10.1016/j.solmat.2013.03.004.

[12] M. Isomura *et al.*, “Microcrystalline silicon–germanium solar cells for multi-junction structures,” *Sol. Energy Mater. Sol. Cells*, vol. 74, no. 1–4, pp. 519–524, Oct. 2002, doi: 10.1016/S0927-0248(02)00069-7.

[13] T. Matsui, M. Kondo, K. Ogata, T. Ozawa, and M. Isomura, “Influence of alloy composition on carrier transport and solar cell properties of hydrogenated microcrystalline silicon-germanium thin films,” *Appl. Phys. Lett.*, vol. 89, no. 14, p. 142115, Oct. 2006, doi: 10.1063/1.2358318.

[14] A. Wilson *et al.*, “Highly Microcrystalline Phosphorous-Doped Si:H Very Thin Films Deposited by RF-PECVD,” *Phys. Status Solidi A*, vol. 219, no. 13, p. 2100876, 2022, doi: 10.1002/pssa.202100876.

[15] G. E. Jellison, M. F. Chisholm, and S. M. Gorbatkin, “Optical functions of chemical vapor deposited thin-film silicon determined by spectroscopic ellipsometry,” *Appl. Phys. Lett.*, vol. 62, no. 25, pp. 3348–3350, Jun. 1993, doi: 10.1063/1.109067.

[16] E. Kadri, K. Dhahri, R. Barillé, and M. Rasheed, “Novel method for the determination of the optical conductivity and dielectric constant of SiGe thin films using Kato-Adachi dispersion model,” *Phase Transit.*, vol. 94, no. 2, pp. 65–76, Feb. 2021, doi: 10.1080/01411594.2020.1832224.

[17] R. Carius, J. Fölsch, D. Lundszien, L. Houben, and F. Finger, “Microcrystalline Silicon-Germanium Alloys for Absorption Layers in Thin Film Solar Cells,” *MRS Proc.*, vol. 507, p. 813, 1998, doi: 10.1557/PROC-507-813.

[18] L. Houben, “Structural properties of microcrystalline silicon-germanium films,” *Philos. Mag. Lett.*, vol. 79, no. 2, pp. 71–78, Feb. 1999, doi: 10.1080/095008399177561.

[19] M. I. Alonso and K. Winer, “Raman spectra of c-SiGe alloys,” *Phys. Rev. B*, vol. 39, no. 14, pp. 10056–10062, May 1989, doi: 10.1103/PhysRevB.39.10056.

[20] O. Pagès, J. Souhabi, V. J. B. Torres, A. V. Postnikov, and K. C. Rustagi, “Re-examination of the SiGe Raman spectra: Percolation/one-dimensional-cluster scheme and ab initio calculations,” *Phys. Rev. B*, vol. 86, no. 4, p. 045201, Jul. 2012, doi: 10.1103/PhysRevB.86.045201.

[21] A. V. Shah *et al.*, “Material and solar cell research in microcrystalline silicon,” *Sol. Energy Mater. Sol. Cells*, vol. 78, no. 1–4, pp. 469–491, Jul. 2003, doi: 10.1016/S0927-0248(02)00448-8.

[22] J. Ni *et al.*, “Microcrystalline silicon–germanium solar cells with spectral sensitivities extending into 1300nm,” *Sol. Energy Mater. Sol. Cells*, vol. 126, pp. 6–10, Jul. 2014, doi: 10.1016/j.solmat.2014.03.029.

[23] L. Yang, J. Newton, and B. Fieselmann, “Raman Spectroscopy of a.SiGe:H Alloys,” *MRS Online Proc. Libr. OPL*, vol. 149, ed 1989, doi: 10.1557/PROC-149-497.

[24] E. Vallat-Sauvain, U. Kroll, J. Meier, N. Wyrsch, and A. Shah, “Microstructure and surface roughness of microcrystalline silicon prepared by very high frequency-glow discharge using hydrogen dilution,” *J. Non-Cryst. Solids*, vol. 266–269, pp. 125–130, May 2000, doi: 10.1016/S0022-3093(99)00769-3.

[25] M. A. Asadabad, M. J. Eskandari, M. A. Asadabad, and M. J. Eskandari, *Electron Diffraction*. IntechOpen, 2016. doi: 10.5772/61781.

[26] Z. C. Holman *et al.*, “Infrared light management in high-efficiency silicon heterojunction and rear-passivated solar cells,” *J. Appl. Phys.*, vol. 113, no. 1, p. 013107, Jan. 2013, doi: 10.1063/1.4772975.

[27] T. Matsui, C. W. Chang, T. Takada, M. Isomura, H. Fujiwara, and M. Kondo, “Thin film solar cells based on microcrystalline silicon–germanium narrow-gap absorbers,” *Sol. Energy Mater. Sol. Cells*, vol. 93, no. 6–7, pp. 1100–1102, Jun. 2009, doi: 10.1016/j.solmat.2008.12.023.